Eco-friendly Electrospun Membranes Loaded with Visible-light Response Nano-particles for Multifunctional usages: High-efficient Air Filtration, Dye Scavenger and Bactericide

Dan Lv[a]，*Ruoxue Wang*[a], *Guosheng Tang*[a]，*Zhipeng Mou*[a]，*Jiandu Lei*[c]， *Jingquan Han*[d], *Stefaan De Smedt*[a,b], *Ranhua Xiong*[a*], *Chaobo Huang*[a,e*]

[a]College of Chemical Engineering, Key Laboratory of Forestry Genetics & Biotechnology, Ministry of Education, Nanjing Forestry University (NFU), Nanjing 210037, P. R. China

[b]Lab General Biochemistry & Physical Pharmacy, Department of Pharmaceutics, Ghent University, 9000, Belgium

[c]Beijing Key Laboratory of Lignocellulosic Chemistry, and MOE Engineering Research Center of Forestry Biomass Materials and Bioenergy, Beijing Forestry University, Beijing, 100083, P. R. China

[d]College of Materials Science and Engineering, Nanjing Forestry University (NFU), Nanjing 210037, P. R. China

[e]Laboratory of Biopolymer based Functional Materials, Jiangsu Co-Innovation Center of Efficient Processing and Utilization of Forest Resources, Nanjing Forestry University, Nanjing, 210037, P. R. China

KEYWORDS: air filtration, antibacterial, electrospinning nanofibers, multifunctional, photodegradation.

ABSTRACT

Ambient particulate matter (PM) pollution has posed serious threats to global environment and public health. However, high efficient filtration of submicron particles, so named 'secondary pollution' caused by e.g. bacterial growth in filters and the use of non-degradable filter materials, remains a serious challenge. In this study, Polyvinyl alcohol (PVA) and konjac glucomannan (KGM) based nanofiber membranes, loaded with ZnO nanoparticles, were prepared through green electrospinning and eco-friendly thermal crosslinking. Thus obtained fibrous membranes do not only show high-efficient air-filtration performance but also show superior photocatalytic activity and antibacterial activity. The filtration efficiency of the ZnO@PVA/KGM membranes for ultrafine particles (300nm) were higher than 99.99%, being superior to commercial HEPA filters. By virtue of the high photocatalytic activity, the Methyl orange (MO) were efficiently decolorized with a removal efficiency of more than 98% at an initial concentration of 20 mgL^{-1} under 120 min solar irradiation. The multifunctional membrane with high removal efficiency, low flow resistance, superior photocatalytic activity and antibacterial activity was successfully achieved. It's conceivable that the combination of biodegradable polymer and active metal particle would form

an unprecedented photocatalytic system, which will be quite promising for environmental remediation such as air filtration and water treatment.

INTRODUCTION:

Air pollution is an unvisitable killer. According to reports of the World Health Organization (WHO), most air pollution-related deaths are from non-communicable disease (NCDs).[1] Indeed, air pollution contributes to stroke, lung cancer, chronic obstructive pulmonary disease, ischaemic heart disease.[1] In addition to the serious effect on human health, particulate matters (PMs) also affect the living environment like visibility that might contribute to climate change etc.[2-5] It all explains why advanced filter techniques to efficiently remove PMs from air are highly desirable.

Fibrous filters such as glass fibers, spun-bonded fibers and melt-blown fibers are widely used in various air filtration devices. However, such fibrous filters usually show low filtration efficiency for fine (submicron) nanoparticles. This sub-optimal filtration performance can be ascribed to the relatively large pores present in such filters, which is due to the use of micrometer sized fibers which may usually show poor uniformity (e.g. low control over the fiber diameter) and low mechanical performance.[6] Nanofiber membranes, made through electrospinning, were introduced to effectively resolve the filtration problems seen for ultrafine particles by virtue of the excellent advantages like a small diameter of the fiber, a controllable porous structure, a high specific surface area, good internal connectivity and steerable morphology.[7-9] To date, various polymers have been successfully fabricated into nanofibrous membranes via electrospinning and evaluated for air filtration, like polyacrylonitrile (PAN),[8] polyethylene oxide (PEO),[10] polyurethane (PU),[11] poly(vinyl alcohol) (PVA),[12] polysulfone (PSU),[10, 13] poly(lactic acid) (PLA),[14] polycarbonate (PC),[15] polyamide (PA)[7] and polyimide (PI)[16] . Most of these electrospun polymer membranes

possess superior filtration performance for ultrathin particulate contaminants. However, so named "secondary pollution", like bacterial growth in the membranes, restricts their use in practical applications. Also, and importantly, fully biodegradable electrospun polymer membranes are needed taking into account the immense challenge of the world faces with the so named 'white pollution', referring to the accumulation of plastics in the environment. As Figure 1 illustrates, multifunctional eco-friendly electrospun polymer membranes with a sufficient thickness, to guarantee a sufficiently high filtration efficiency, are needed. Though, thicker membranes inevitably result in a higher pressure drop over the filter which means a higher energy cost to filtrate air. To overcome these shortcomings, researchers have been looking for innovative strategies in recent years. For example, the exploitation of green chemistry to make electrospun nanofiber membranes,[17-20] the use of bio-originated and biodegradable polymers, and also nanofiber membranes which are loaded with active components.[21-25]

Inspired by the earlier work, the nature polymer konjac glucomannan (KGM) and active metal oxide ZnO nanoparticles were induced with water-soluble polymer PVA to form uniform electrospun nanofibers membrane. As pure PVA and KGM nanofibers immediately dissolved upon contact with water which seriously restricted their application. The citric acid (CA) was introduced as the crosslinking agent to improve their mechanical properties. Compared with synthetic polymers, natural polymers are readily available, biocompatible and biodegradable. KGM as the natural polysaccharide, is well known to have more efficient physical and chemical properties, such as good water absorption and film-forming ability, as well as bioactivity.[26-27] To enhance the performance of the composite membrane and expand more functions, the incorporation of metal oxides was proposed earlier by our group.[12] Among existing active metal oxides, ZnO is nearly ideal material in terms of the optical, electrical, chemical and biological

properties.[28] For that purpose, nano-sized ZnO is an ideal metal oxide as it is biocompatible while it also shows photocatalytic and antibacterial activity.[29-30] Indeed, as e.g. industrial waste water is often polluted with organic dyes, it is highly desired to degrade these refractory organics[31]. In the present work, the biocompatible and biodegradable blend of PVA and KGM electrospun nanofibrous membranes loaded with active ZnO nanoparticles (ZnO@PVA/KGM) were successfully prepared via green electrospinning and eco-friendly thermal crosslinking (Figure 1a**)**. Thus, it is conceivable that the combination of electrospun-synthesized nanofibrous membrane and the photoactive nano-ZnO particles would form an unprecedented photocatalytic system with specific functions for air filtration (Figure 1b), photodegradation (Figure 1c), and bacteriostasis (Figure 1d).

EXPERIMENTAL METHODS

2.1 Materials

Poly(vinyl alcohol) (PVA-124, 98–99.8% hydrolyzed), agar powder and beef extract were purchased from Sinopharm Chemical Reagent Co., Ltd., China. Konjac glucomannan (KGM, Mw~900 000, 95%) was obtained from Jiangsu Boyao Bio-tech Co., Ltd. (Jiangsu, China) and Zinc oxide (ZnO, 30±10nm) were purchased from Shanghai Macklin Biochemical Co., Ltd. Citric acid (CA, GR 99.8%) was purchased from Aladdin (Shanghai, China). Peptone was supplied by Beijing Aoboxing Bio-tech Co., Ltd., (Beijing, China). Sodium chloride was purchased from Xilong Chemical Co., Ltd., China. All of the chemicals noted above were used as received. All solutions were prepared with ultrapure water (Laboratory water purified device, Nanjing Qianyan Instrument Equipment Co., Ltd., China).

2.2 Preparation of the ZnO@PVA/KGM nanofiber membranes

Preparation of the ZnO@PVA/KGM solution for electrospinning

The PVA solution (10 wt %) was prepared by dissolving 10 g PVA in 90 ml ultra-pure water and then stirred at 85 °C for 4 h. 1 g KGM was dissolved in 9 g ultra-pure water and stirred at room temperature for 1 h (1 wt % KGM solution). PVA/KGM solutions were obtained by mixing the PVA and KGM solutions in different weight ratio (9:1, 8:2, 7:3, 6:4, 5:5) followed by stirring for 2 h at room temperature. Details about the optimization experiment are provided in supporting information. PVA/KGM solutions (weight ratio 8:2) containing 0.06, 0.08, 0.1, 0.2, 0.4, and 0.6 wt % citric acid (CA) were prepared as well. The ZnO nanoparticles of different weight ratio (0, 0.5, 1.0, 1.5, 2.0 wt%) were dispersed in ultra-pure water and further mixed with PVA and KGM to form the composite precursor solution. All the solutions were further stirred (ultrasonic stirring; 40 kHz) for 2 hours at room temperature to form the homogenous blend electrospinning solution.

Fabrication of ZnO@PVA/KGM nanofiber membranes by electrospinning

The nanofiber membranes were fabricated using commercially available electrospinning equipment (FM1206, Beijing Future Material Scitech Co., Ltd., China). PVA/KGM solutions (see above) containing ZnO nanoparticles (0, 0.5, 1.0, 1.5, and 2.0 wt %) were prepared. Typically, ZnO@PVA/KGM dispersions were transferred into a 5 mL plastic syringe attached to a capillary tip with an inner diameter of 0.7 mm and pumped out at the rate of 0.66 mL/h. An electric potential of 18 kV was supplied to the metal needles to form charged liquid jets, upon rapid evaporation of the solvent, turned into nanofibers on the collector of the instrument (the distance between the capillary tip and the fiber collector was 15 cm). All the nanofibers were deposited on the nonwoven

substrate (15 cm × 15 cm) that overlaid on a grounded metal roller (diameter of 12 cm) rotated at a speed of 50 rpm. To guarantee uniform membranes, the injection pump was set to move horizontally backward and forward at a speed of 20 cm/min over a distance of 2 cm. The temperature and relative humidity in the laboratory were 25 ± 2 °C and 40 ± 2 %, respectively. After electrospinning, all the samples were dried (vacuum-drying at 60 °C for 1 h) to remove the residual solvent. Then membranes were subsequently subjected to vacuum drying at 140 °C for 2 h to complete the esterification reaction (thermal crosslinking). After thermal crosslinking, esterification occurs between respectively the hydroxyl groups of PVA and KGM and the carboxyl groups of CA (Figure 1a).

2.3 Resistance of PVA/KGM nanofiber membranes to water

The pre-crosslinked membrane was cut into 2 × 2 cm^2 and the weight of the small film was measured, then immersed in 50 mL distilled water at room temperature, and soaked for 24 hours. After 24 hours' soak, the membrane was dried (vacuum freeze-drying, -48 °C, 12 hours) and the weight of the membrane was measured. The degree of crosslinking can be quantitatively analyzed by the weight loss rate. The weight loss of the membranes (%) upon dispersing them in water was calculated from the equation below[32]:

$$W(\%) = \frac{M_1 - M_2}{M_1} \times 100 \quad (1)$$

Where M_1 is the initial weight of the membrane, M_2 is the weight of membrane after 24 h immersing in water and subsequently dried.

2.4 Air filtration tests

The filtration performance of the membranes was evaluated using the LZC-H filter tester (Huada Filter Technology Co., Ltd., China, details are provided in Figure S1). The detailed filtration measurements for the composite membrane were presented in supporting information. The durability and reused performance were determined by testing the membrane for more than 30 cycles and 300 minutes. A membrane (10×10 cm^2 effective area) was placed on the filter bracket. The filter tester made use of di-iso-octyl sebacate (DEHS) and neutral monodisperse NaCl particles as aerosol particles (diameter ranged from 300 nm to 10 μm). The neutralized NaCl and DEHS aerosol particles were transported, upwards and downwards, through the membranes.[12] A flow meter was used to adjust the air flow which was set as 32 L/min in our experiments. The removal efficiency can be calculated by detecting the number of airborne particles in the upstream and downstream of the airflow, which could be calculated from the equation $\eta = 1-\varepsilon_1/\varepsilon_2$, where ε_1 and ε_2 represented the quantities of aerosol particles in the downstream and upstream of the filter, respectively.[33] The pressure drop over the upstream and downstream sides of the membrane was measured by a flow gauge and two electronic pressure transmitters as shown in Figure S1, supporting information. Each membrane was tested three times. The quality factor (QF), a widely used parameter to appraise the filtration performance of filters, was calculated by Eq (2), where η is the removal efficiency of the membrane and Δp is the pressure drop over the membrane filters.

$$QF = -\frac{\ln(1-\eta)}{\Delta p} \quad (2)$$

2.5 Photocatalytic activity tests

It was aimed to investigate the role of the ZnO nano-particles loaded on the electrospun membrane and their influence on the degradation of Methyl orange (MO). A 50 ml Methyl orange

(MO) solution (20 mgL^{-1}) was initially taken for the photocatalytic studies. The photocatalytic degradation of MO was carried out in a 100ml cylindrical photo-reactor. Upon irradiation light intensity equaled 83 $mW\,cm^{-2}$ (solar simulator;300 W Xenon lamp, CEL-HXF300). The MO samples were collected every 5 minutes at the first 35 minutes and every 10 minutes then from the suspension and filtered by the MO-saturated Whatman filter to remove the catalyst before further analysis. Prior to irradiation, the solution was stirred in dark for 120 minutes to achieve the adsorption-desorption equilibrium. The MO concentrations were measured by the UV–vis diffuse reflectance spectra (DRS) spectrophotometer (UV-2600, Shimadzu, Japan) at the maximum absorption wavelength (λ) of 462 nm. The MO removal efficiency (Ɛ%) of photocatalytic degradation of MO was calculated using Eq. (3); where C_0 and C are the initial and final concentrations of the MO solution.

$$Ɛ(\%) = \frac{C_0 - C}{C_0} \times 100\,\% \qquad (3)$$

2.6 Testing the antibacterial activity of the ZnO@PVA/KGM membranes

An agar solution was poured into a disposable sterile culture dish and allowed to solidify. A suspension of Gram-negative (*E. coli*) and Gram-positive bacteria (*Bacillus subtilis*) was uniformly applied on the agar plate, respectively. Electrospun nanofiber membranes were cut into circular films (diameter of 8mm). The circular films were aseptically manipulated with sterile forceps and gently pressed to bring them into intimate contact with the solid medium. The culture dishes were subsequently incubated at 37 ℃ for 24 hours. The antibacterial activity of the ZnO@PVA/KGM membranes was estimated from the area in which bacterial growth was inhibited (‘inhibition zone’), using ImageJ.

2.7 Characterization

The surface morphology and EDS spectra of the membranes was studied by field emission scanning electron microscopy (FE-SEM, S-4800, Hitachi Ltd., Japan). The surface of the ZnO-loaded filters was analyzed using an X-ray photoelectron spectrometer (XPS) (AXIS Ultra DLD, UK). The extent of cross-linking in the fibers was determined from fourier transform infrared (FT-IR) spectra (Nicolet 8700 FT-IR spectrometer). The thermal stability of the membranes was evaluated with a Thermal Gravimetric Analyzer (TGA Q5000-IR, TA Instruments). The mechanical properties were characterized by a Sans UTM6502 universal testing machine (Shenzhen, China). The leached quantity of the ZnO was analyzed by inductively coupled plasma atomic emission spectroscopy (ICP-MS, Perkin Elmer Nixon 300X). Fluorescence photographs of the composite membranes were taken using a Laser Scanning Confocal Microscope (Carl Zeiss, LSM710). The pore size distribution was conducted by surface area and porosity analyzer at 77 K (Quantachrome BET instrument, Quantachrome Corporation, USA).

3 RESULTS AND DISCUSSION

3.1 Water resistance of PVA/KGM nanofibrous membranes

As pure PVA nanofiber immediately dissolve when contact with water. Incorporating with plasticizers, crosslinking agents or hybrid with other natural polymers can effectively improve the properties. Here, the nature-originated polymer KGM was selected to electrospun with water-soluble polymer PVA to form the uniform nanofiber membrane in this work. CA as the crosslinking agent was added into the hybrid PVA/KGM solution. The optimum proportion of

additives were determined by initial screening tests and hydrolysis-resistant experiment (supporting information).

Initial screening experiments with PVA/KGM solutions (varying in PVA/KGM composition) revealed that PVA/KGM solution with a weight ratio of 8:2 could generate uniform nanofibers (Table S1). Subsequently PVA/KGM-CA solutions (varying in CA-concentration) were electrospun into fibers. These nanofibers were then thermally treated to complete the crosslinking process. Thus obtained membranes were immersed in water for 24 h and subsequently dried. Figure 2a shows that the weight loss of the membranes (upon dispersing them in water) could significantly prevented when a sufficiently high concentration of CA was used (0.6 wt %). Figure 2d shows that the membranes with low amounts of CA became severely swollen and deformed when immersed in water. Using higher amounts of CA significantly improved the resistance to water; with 0.6 wt % of CA, the morphology of the nanofiber membranes did no longer change after being in contact with water for 24 hours as shown in Figure 2d (I-VI).

Upon thermal treatment, esterification should occur between respectively the hydroxyl groups of PVA and KGM and the carboxyl groups of CA (Figure 1) after the 140℃ heat treatment. Which could readily overcome the inherent hydro instability, thus making previously water-soluble material to insoluble material. FT-IR measurements (Figure 2c**)** indeed confirmed the thermal crosslinking of the PVA/KGM-CA nanofiber membranes. The large bands around 3320cm^{-1} correspond to the -OH stretching of intramolecular and intermolecular hydrogen bonds; bands at 2940 cm^{-1} and 852 cm^{-1} are the backbones of -CH_2 symmetric stretching vibration and out-of-plane twisting; the small bands at 1097 cm^{-1} correspond to "-C-O". It can be seen that the stretching vibration of "-C=O" (1700 cm^{-1}) becomes stronger after thermally crosslinking, which means that the "-C=O" stretching vibration (1720 cm^{-1}) is normally shifted to the right through

esterification. Also, the -OH groups absorption peak (at 3400 cm^{-1}) becomes weak, all proving that the esterification crosslinking reaction was successfully conducted. Further, the mechanical properties of the pure PVA membrane and PVA/KGM composite membrane before and after crosslinking were characterized, as shown in Figure 2b. It is found that the KGM itself could obviously enhance the mechanical strength of the membrane. After the crosslinking treatment, the mechanical performance of the membrane significantly improved which further confirmed that the crosslinking process not only endow the membrane with water resistance but also improve the mechanical properties.

3.2 PVA/KGM nanofiber membranes loaded with ZnO nanoparticles

We applied SEM to visualize surface morphology of ZnO@PVA/KGM membranes. As Figure 3a shows, electrospun nanofibers were uniformly distributed, while ZnO nanoparticles were not observed; it suggests that, due to their small size (30±10 nm), the ZnO nanoparticles were encapsulated by the nanofibers (diameter > 100 nm; see further). Meanwhile, as shown in Figure 3b and Table S3, we took advantage of Energy Dispersive Spectrometry (EDS) to determine the characteristics of the ZnO features on the fibers, results confirmed that the ZnO were successfully loaded in the membrane. Surface characterization of the ZnO@PVA/KGM composite membrane was analyzed by X-ray photoelectron spectrometer (XPS). Figure 3c shows that two well separated peaks of ZnO $2P_{3/2}$ and Zn $2p_{1/2}$ could be observed at 1021 eV and 1044 eV, respectively. These proved that the ZnO particles was relatively stable in oxidation. Fluorescence photographs were obtained by Laser Scanning Confocal Microscope. As shown in Figure S2 (a)and (b), the ZnO nanoparticle loaded in the fibers endow the whole fiber emitting a bright fluorescent glow, indicating that ZnO nanoparticles were attached and dispersed uniformly in the fiber since the

fluorescence is continuous and uniform. The combination of both ZnO nanoparticles and the nanofibers was studied by leaching test (supporting information). The ICP measurements results (Table S2) showed that the concentrations of leached ZnO in water were relatively low after continuously shaking, indicating that there are good attachments between the ZnO nanoparticles and the nanofibers. Based on these results, it could be confirmed that the electrospun process enables the direct formation of densely structured ZnO features onto the filter fibers. The thermal stabilities of ZnO nanoparticles loaded nanofibrous membrane were investigated by the thermogravimetric analyzer (TGA) from 30 ℃ to 800 ℃ (under nitrogen atmosphere). As shown in Figure 3d, there are little weight change before 100℃, which may be due to the slight dehydration of PVA and KGM under heating conditions. Degradation of the ZnO@PVA/KGM nanofibrous membrane started around 300 ℃ followed by a fast degradation at higher temperatures, then the curve of weight percentage fast drop. This may be attributed to the degradation of the polymer framework. With the increase of temperature, the weight percentage slowly decreased after 500 ℃ and tend to be stabilized. Interestingly, we found that the thermal stability of these ZnO@PVA/KGM composite electrospun nanofibrous membranes increases with the increasing of ZnO amount. Which means the ZnO@PVA/KGM composite membranes is seized of a good thermal stability at temperature up to 300°C, which can be applicable in some middle-temperature environment.

3.3 Filtration performances of ZnO@PVA/KGM nanofibrous membranes

The SEM images presented in Figure 4a show a typical surface morphology of the ZnO@PVA/KGM nanofibrous membrane (1.0 wt% ZnO) before and after a filtration test. To further enhance the filtration performance of the blend PVA/KGM fibrous filter, the nano-sized

ZnO particles were added into the PVA/KGM system by electrospinning the mixture of ZnO and PVA/KGM solution into fibrous membrane. To explore the role of ZnO nanoparticles loaded on nanofiber membranes, the filtration efficiency of the green electrospun nanofiber membrane with different ZnO concentration for various particle diameter from 0.3μm to 10μm were systematically investigated under the designed air flow of 32 L/min, as shown in Figure 4b and Table S4. The filtration efficiency showed an improved trend with the increase of ZnO concentrations, which could be attributed to the increased surface roughness and specific surface area that played a dominant role in the particle intercept of the ZnO@PVA/KGM membrane. Since filters always show relative low filtration efficiency for submicron particles, here the filtration efficiency mentioned are for 0.3μm particles. Although the membrane without ZnO could achieve a high removal efficiency level of >97%, with the increasing ZnO content from 0 wt% to 1.0 wt%, the filtration efficiency further increases from 97.07% to 99.99%. Meanwhile we found its pressure drop increased accordingly from 89.0 Pa to 130.0 Pa as shown in Figure 4c and Table S4. Interestingly, the filtration efficiency further decreased to 98.01% (pressure drop increased to 158Pa) when the ZnO concentration increased from 1.0 wt% to 2.0 wt%, which could be ascribed to the poor spinnability of the precursor solution caused by high ZnO concentration. This suggest that an unreasonable trade-off design for practical application: slightly enhanced efficiency at the expense of hugely increased pressure drop. Based on the QF value (Figure S3), the nanofiber membranes which contain 1.0 wt % ZnO were selected as being the most optimum condition take both of the filtration efficiency (99.99%) and pressure drop (130Pa) into consideration. It is worth noting that the filtration efficiency almost approaching to 100% when the diameter of the particles is larger than 1μm, furthermore, which could maintain 100% filtration efficiency for particles with a diameter of 5μm and 10μm (PM_{10}).

We further investigated the pore size and pore distribution of the composite membranes with ZnO content of 0, 0.5, 1.0, 1.5 and 2.0 wt%, respectively (Figure S4). The ZnO@PVA/KGM membranes showed the pore sizes distribution in the range of 0.6-25 nm and single pore distribution peak, thus confirming that the membranes possessed uniform-and relatively narrow pore distribution. It is worth noting that the pore size decreased with increasing the ZnO contents. Moreover, the cumulative pore size distributions of membranes with 1 wt% ZnO presented that most of the pores are concentrated between 2.4 and 4.9 nm. SEM imaging also revealed that diameter (distribution) of the fibers depended on the ZnO concentration. Further systematically investigation of the fiber diameters was carried out by the ImageJ software, the diameter distributions were presented in Figure S6. To analyze the diameter distribution varied with ZnO concentration, the fiber diameters of different ZnO concentrations were analyzed by the mathematical statistics software SPSS (supporting information), and the results are presented in the box chart (Figure 4d), where data points are the mean and the standard deviations of samples. Results turned out that there is a significant difference between different ZnO concentration. Compare to the ZnO@PVA/KGM (1wt%) membranes, the fibers with the other percentage of ZnO have a large diameter size in a much broad diameter distribution. This further strongly confirmed the highest filtration efficiency and relatively low pressure drop were found in 1.0 wt% ZnO composite membrane.

To further investigate the reused performance and durability of the ZnO loaded hybrid PVA/KGM electrospun nanofibers membrane, the filtration efficiency of the membrane (1.0 wt% ZnO) was tested for 30 cycles (Figure 4e) and 300 minutes (Figure S5). The membrane could maintain more than 97% filtration efficiency even after 150 minutes (Figure S5). Obviously, the ZnO@PVA/KGM nanofibrous membrane could be reused as many as 30 cycles with the filtration

efficiency maintained more than 98% for 0.3μm particles (still maintain 100% for 5μm and 10μm particles). As the inset SEM images shown in Figure 4e, the particle matters were adhered closely to the fibers in the surface of the filtration membrane. This phenomenon can be explained by that, the larger particles were intercepted by the fibers during the filtration process while the few extremely small ones maybe crashed into the nanofiber porous and tightly adhered by virtue of the Van der Waals force.[34]

3.4 The photocatalytic activity of ZnO@PVA/KGM nanofiber membranes

ZnO has been proven to be efficient for photocatalysis (band gap: 3.37 eV at room temperature).[35-36] The photocatalytic degradation mechanism of ZnO is illustrated in Figure 5a: when ZnO is irradiated by photons with an energy level exceeding its band gap, energy excites electrons (e^-) from the valence band to the conduction band, and holes (h^+) are generated in the valence band; strong oxidant hydroxyl radical (·OH) can be generated by reaction between the photo-generated valence band holes and water (H_2O) or hydroxyl ions (OH^-), adsorbed on the surface of the catalyst. The photo-generated electrons in conduction band may react with oxygen(O_2) to form the superoxide ions ($\cdot O_2^-$) which can further react with water to produce hydrogen peroxide (H_2O_2) and hydroxyl ions(OH^-). The degradation of organic dye can be realized through the reaction with hydroxyl radicals (·OH) or direct attack from the valence band holes.

The photocatalytic performances of ZnO loaded PVA/KGM electrospun membranes were evaluated from the reduction of MO, which is a typical highly colored, non-biodegradable and toxic refractory organic dye. Photocatalysis experiments were carried out by nanofiber membranes with and without ZnO nanoparticles (control samples) using a 300 W Xenon lamp. It is noting that the membrane used here was loaded with 2.0 wt% ZnO, expect where noted. The samples are

collected from the reactor at various exposure time. Prior to illumination, the solution was kept in dark for 120 min stirring to reach an adsorption-desorption equilibrium. Absorption measurements on MO solutions revealed that exposing the MO solutions (during 2 hours) to respectively light and membrane without ZnO, light (only), ZnO (only) and the combination of light and ZnO loaded membranes decreased respectively 9, 15, 17 and 98% of the initial concentration, clearly indicating that the co-treatment with ZnO loaded membrane and visible light significantly promoted the degradation (Figure 5b). A typical UV-vis spectra result of the MO solutions are presented in Figure 5c, a decrease in the peak intensity with time shows that the MO dye were efficiently decreased and the catalysts were photoactive. To further investigate the changes of the MO solutions, the max absorbance of MO in the typical UV-vis spectra is presented in Figure 5d. It was obvious that the MO concentration was significantly reduced and the absorbance of MO almost trend to 0 after 35 minutes light irradiation. As shown in Figure 5e, the MO color obviously changed after light irradiation and the degradation efficiency almost reached 98% after 120 minutes by virtual of solar irradiation and photocatalyst ZnO. Finally, we can conclude that nano-sized ZnO particles could noticeably enhance the photocatalytic activity of the composite membranes.

3.5 Antibacterial activity of the ZnO@PVA/KGM membranes

The active ZnO nanoparticles possesses good biocompatibility, superior safety, and long term effect. ZnO could show excellent antibacterial properties in the absence of light, even at low concentration. Here, the antibacterial active of the ZnO loaded PVA/KGM electrospun nanofibrous membranes were investigated by both *E. coli* and *Bacillus subtilis*. As shown in Figure 6 (a) and (b), the ZnO@PVA/KGM nanofibrous membranes showed obvious antibacterial

activities against both *E. coli*, and *Bacillus subtilis* compared to the control samples (without ZnO nanoparticles). A general trend could be obtained; the antibacterial performance could be enhanced significantly with the increasing of ZnO concentration. To quantitative analysis the antibacterial performance of the electrospun ZnO loaded nanofibers membrane, the diameter of the bacteriostatic ring was measured and analyzed as shown in Figure 6c. The highest antibacterial activity for both *E. coli* and *Bacillus subtilis* was found in 1.0 wt% and 2.0 wt% ZnO@PVA/KGM, respectively. However, we interestingly found when the ZnO content is over 1.0 wt%, the antibacterial activity for *E. coli* did not increase but decreased. Highly like this can be explained by the fact that the ZnO nanoparticles could be uniformly dispersed over the membrane surface when the ZnO concentration was 1.0 wt%. While when the concentration increased over 1.0 wt% and reached a higher concentration, the spinnability of the blend solutions were markedly reduced and the ZnO are gathered into clusters and adhered into the fibrous membranes, randomly. Compared to the membrane uniformly dispersed with ZnO nanoparticles, the membrane with random ZnO cluster (maybe somewhere without) shown lower antibacterial activity may be entirely persuasive.

CONCLUSION

We proposed a new method of eco-friendly crosslinked blend PVA/KGM electrospun nanofibers membrane loaded with ZnO nanoparticles. The strategy of thermal cross-linking significantly improved the water resistance and mechanical properties of the Polyhydroxyl water-soluble polymer. Besides, the introduction of active ZnO nanoparticles don't only remarkably improved filtration efficiency but also endow the ZnO@PVA/KGM membrane with photocatalytic activity and antibacterial activity. The composite membrane presents a superior

filtration efficiency to commercial HEPA filters, a high photocatalytic degradation efficiency of more than 98% and a superior antibacterial activity against both Gram-negative (*E. coli*) and Gram-positive bacteria (*Bacillus subtilis*). For the above-mentioned superiorities, we expect that such multifunctional nanofiber membranes will be greatly helpful for reducing environmental contamination by the air filtration systems and photocatalytic degradation feature as well as the antibacterial performance.

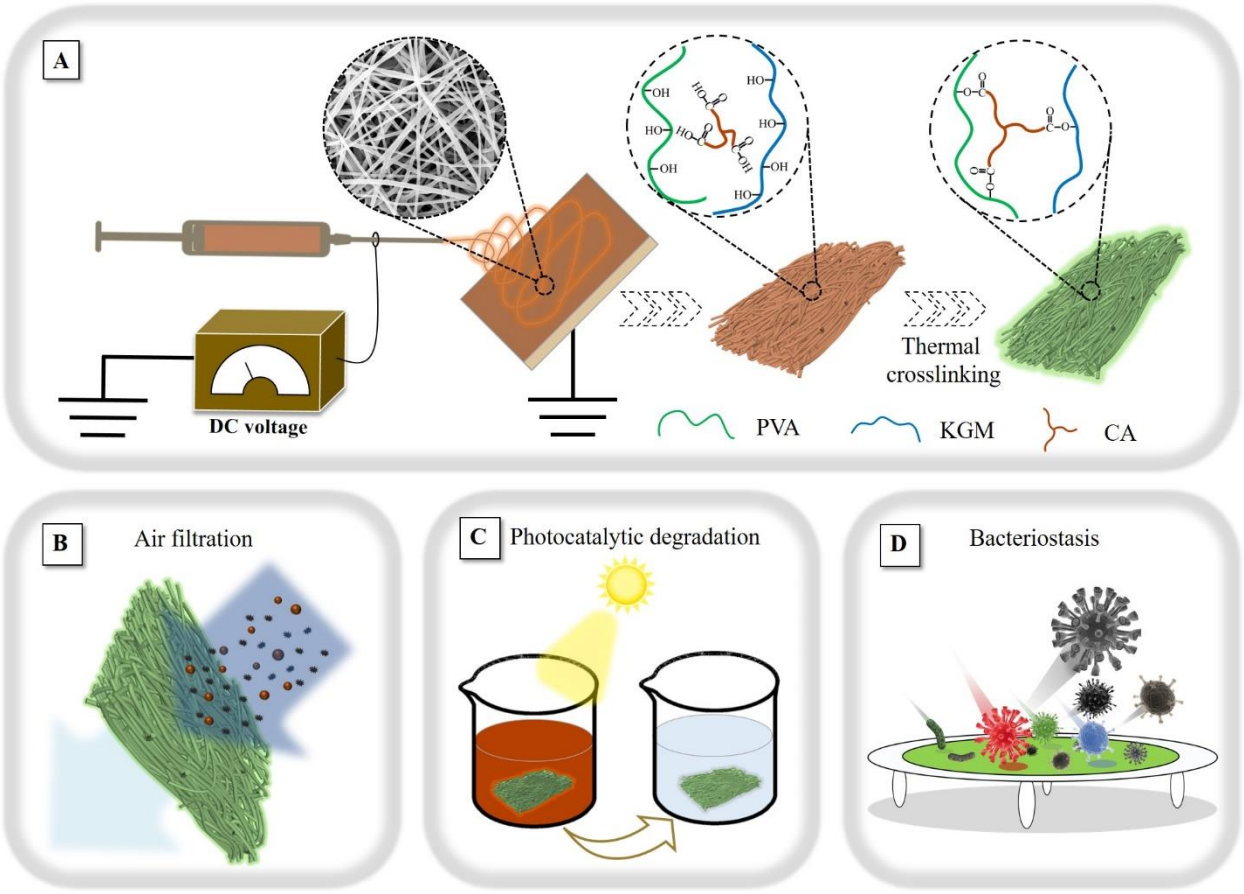

Figure 1. Multifunctional ZnO@PVA/KGM electrospun nanofiber membranes. (a) Schematic presentation of the preparation of the membranes by electrospinning and their application for (b) air filtration; (c) illustrates photocatalytic degradation while (d) illustrates the antibacterial activity of the membranes.

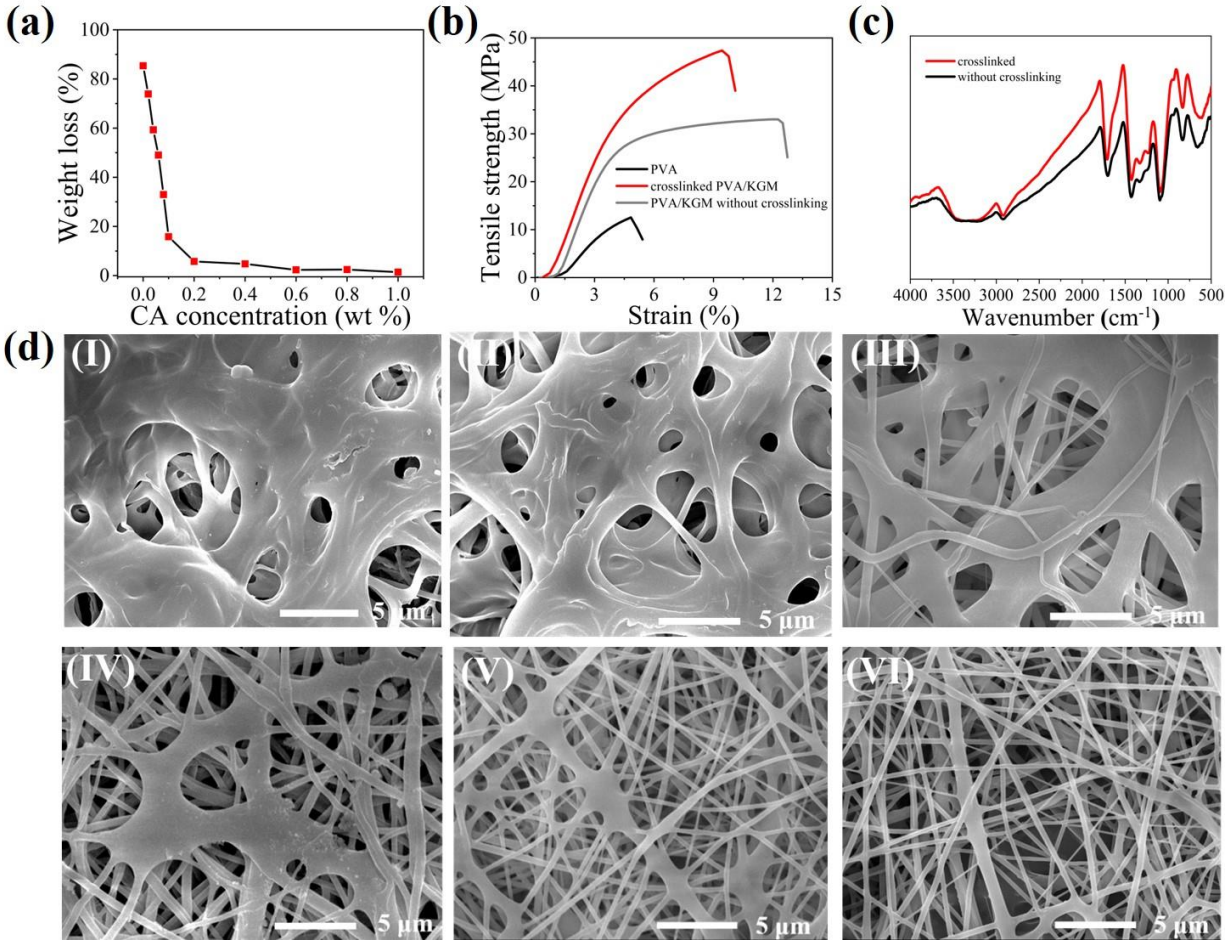

Figure 2. Water resistance of the thermally cross-linked PVA/KGM nanofiber membranes. (a) Weight loss of the membranes after 24h immersion in water; note that the CA concentration varied. (b) Mechanical properties of the membranes (c) FT-IR spectrum of the membranes before and after thermal crosslinking. (d) FE-SEM images of the membranes after 24 h in water. The CA concentration varied from 0.06 (I), 0.08(II), 0.1(III), 0.2(IV), 0.4(V) to 0.6 (VI) wt %, respectively.

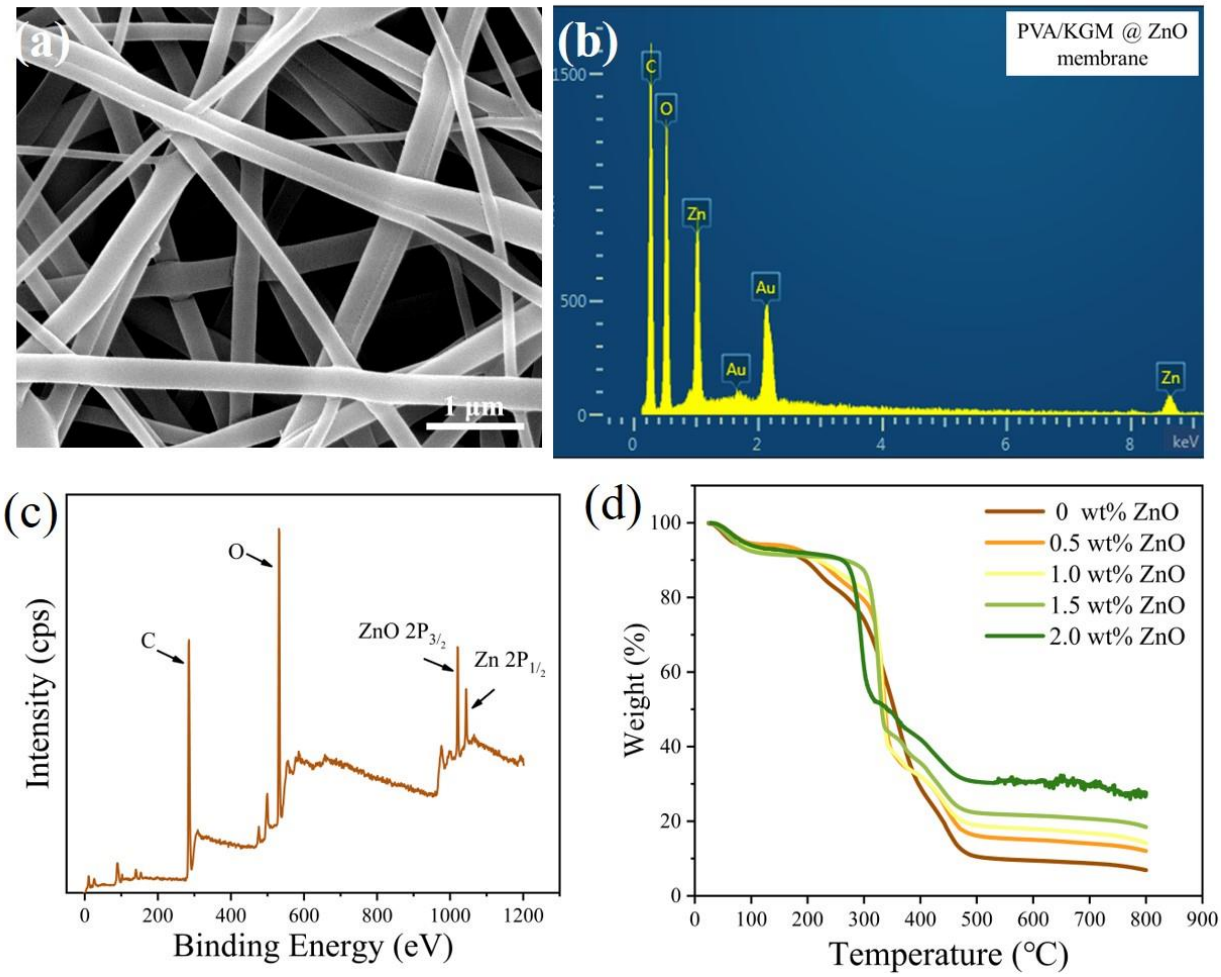

Figure 3. Characterization of the ZnO@PVA/KGM nanofiber membranes. (a) SEM image of a ZnO loaded membrane. (b) EDS and (c) XPS images of ZnO@PVA/KGM nanofiber membranes (2.0 wt% ZnO). (d) TGA on membranes with different ZnO concentrations.

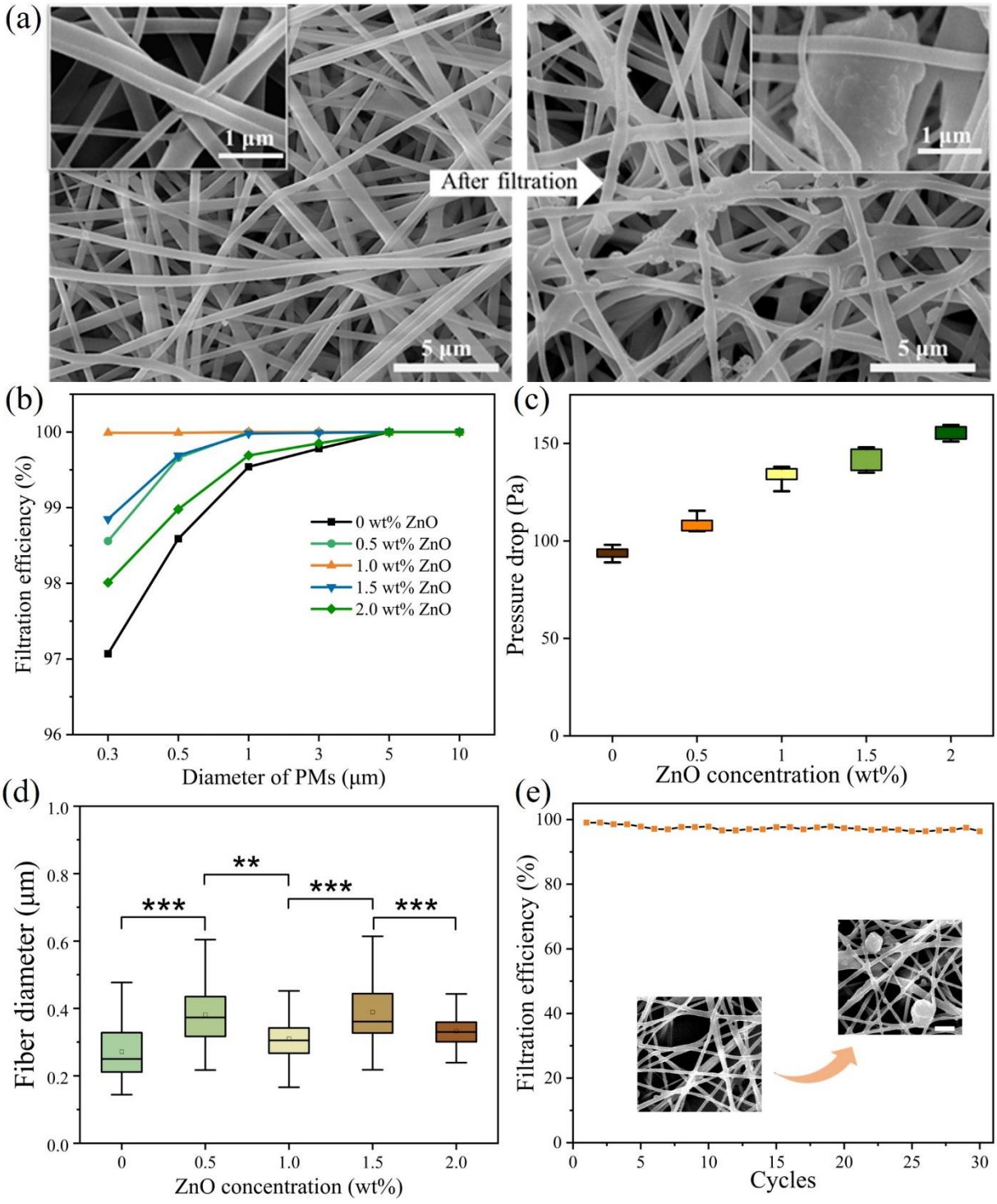
(a)
1 μm
After filtration
5 μm
1 μm
5 μm
(b)
Filtration efficiency (%)
Diameter of PMs (μm)
0 wt% ZnO
0.5 wt% ZnO
1.0 wt% ZnO
1.5 wt% ZnO
2.0 wt% ZnO
(c)
Pressure drop (Pa)
ZnO concentration (wt%)
(d)
Fiber diameter (μm)
ZnO concentration (wt%)
**
***
***
***
(e)
Filtration efficiency (%)
Cycles

Figure 4. Filtration performance of the ZnO@PVA/KGM electrospun membranes (1.0 wt% ZnO). (a) SEM images of the nanofiber membrane before (left) and after (right) filtration. (b) Removal efficiency (η in equation 2) of the membranes varying in ZnO concentration (a constant air flow of 32 L/min was used). (c) The pressure drop measured over membranes loaded with different ZnO concentrations (the aerosol particle diameter in the experiments was 300nm). (d) The diameter (distribution) of the fibers (as measured from EM images, using Image J software). (e) The removal efficiency of the membranes after multiple filtration cycles; SEM images of the membranes, the scale bar is 2 μm. (* $P<0.05$, **$P<0.01$, *** $p<0.001$).

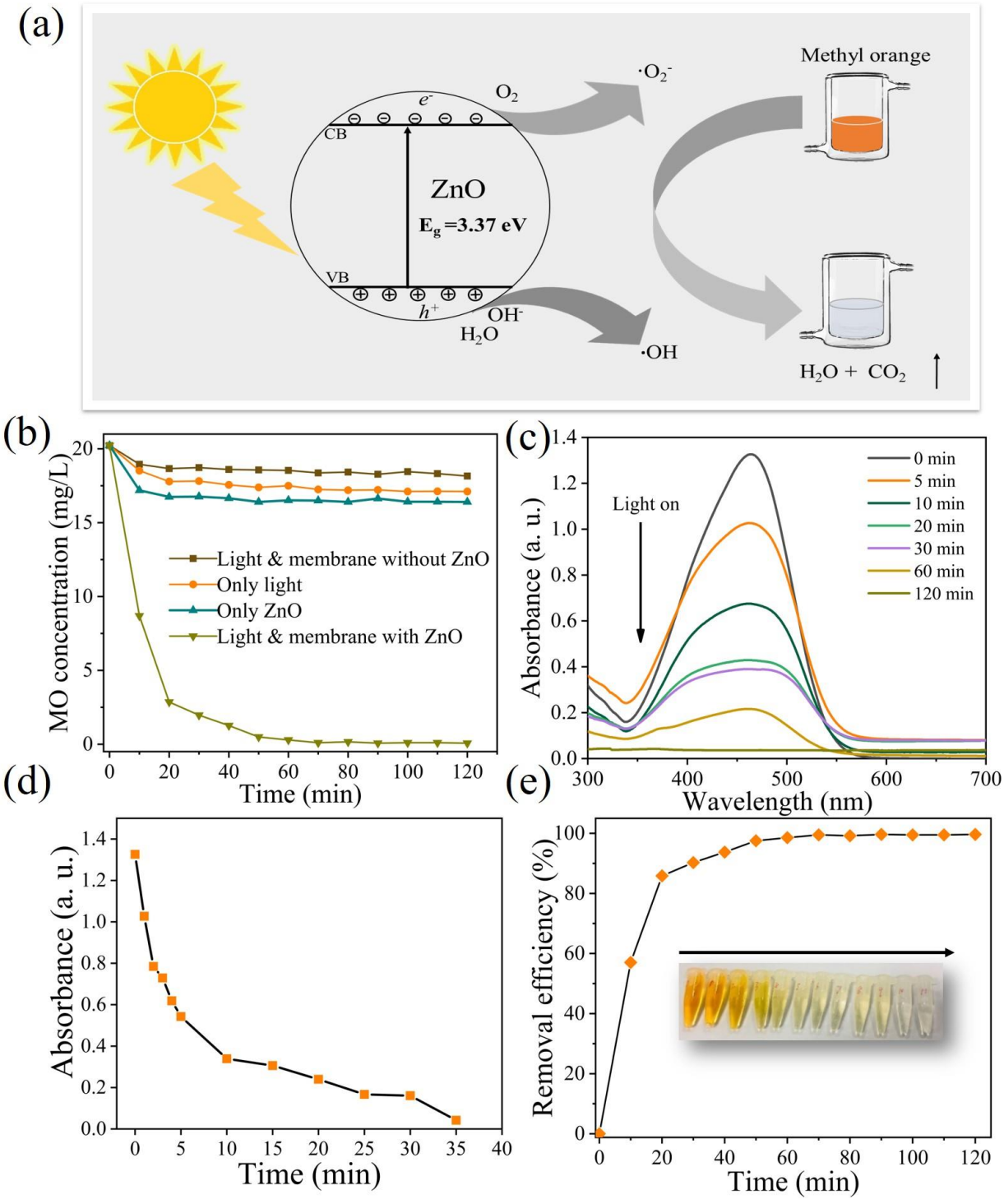
(a)
Methyl orange
O_2
$\cdot O_2^-$
e^-
CB
ZnO
E_g=3.37 eV
VB
h^+
OH^-
H_2O
$\cdot OH$
$H_2O + CO_2$
(b)
MO concentration (mg/L)
Time (min)
Light & membrane without ZnO
Only light
Only ZnO
Light & membrane with ZnO
(c)
Absorbance (a. u.)
Wavelength (nm)
Light on
0 min
5 min
10 min
20 min
30 min
60 min
120 min
(d)
Absorbance (a. u.)
Time (min)
(e)
Removal efficiency (%)
Time (min)

Figure 5. Photocatalytic active of the ZnO loaded membranes. (a) Illustration of the mechanism of the photocatalytic degradation of Methyl orange. (b) MO concentration as a function of time under various conditions i.e. exposing the MO solution to respectively (only) light, (only) ZnO loaded membranes, light and membrane without ZnO, and the combination of light and ZnO loaded membranes. (c) Adsorption spectra of MO solutions exposed to ZnO loaded membranes and light. (d) The absorption (λ = 464 nm) of the MO solution as a function of time. (e) The MO removal efficiency of the membrane as a function of time; the inset shows the gradual decoloring of the MO solution.

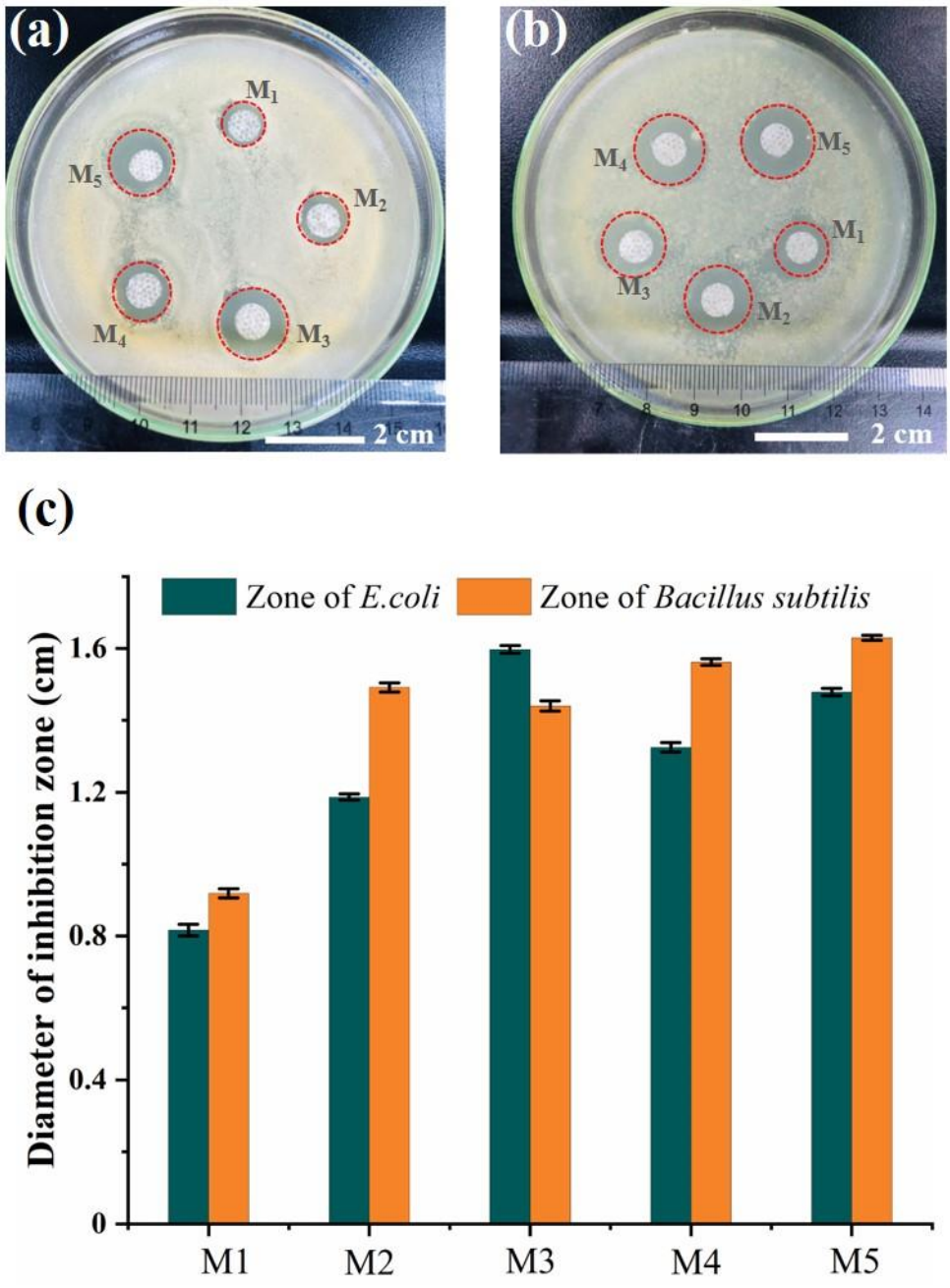

Figure 6. Antibacterial activity of ZnO@PVA/KGM nanofiber membranes against (a) *E. coli* and (b) *Bacillus subtilis*. M1-M5 correspond to membranes loaded with varying amounts of ZnO (0, 0.5, 1.0, 1.5 and 2.0 wt%, respectively). (c) Diameter of the inhibition-zones as a function of the weight percentage of ZnO in the membranes.

ASSOCIATED CONTENT

Supporting Information.

Initial screening experiments and hydrolysis-resistant tests, leaching test, filtration measurement of the fibrous membrane, statistical analysis, characterization of pore size and its distribution, optical photograph and schematic diagram of the filtration tester, confocal microscopy images of the electrospun membranes, QF of the ZnO@PVA/KGM nanofiber membranes, pore size distribution of the composite membranes, filtration performance of the composite membrane over time, FE-SEM images of ZnO@PVA/KGM composite membranes and the diameter distribution of the fibers, EDS data of the composite membrane with 2.0 wt% ZnO nanoparticles, leaching test results of ZnO nanoparticles, filtration performance of the composite membranes. This material is available free of charge via the Internet at http://pubs.acs.org.

AUTHOR INFORMATION

Corresponding Author

*Email: huangchaobo@njfu.edu.cn

* Email: ranhua.xiong@gmail.com

Notes

The authors declare no competing financial interest.

ACKNOWLEDGMENT

National Natural Science Foundation of China (No. 21774060, 31770609), National Key R&D Program of China (2017YFF0207800), Jiangsu key lab of biomass-based energy and Materials (JSBEM2016011), State Key Laboratory for Mechanical Behavior of Materials (20171914),

Priority Academic Program Development of Jiangsu Higher Education Institutions (PAPD), Top-notch Academic Programs Project of Jiangsu Higher Education Institutions (TAPP) and Natural Science Key Project of the Jiangsu Higher Education Institutions (16KJA220006) are acknowledged with gratitude. We also thank Advanced Analysis & Testing Center, Nanjing Forestry University for SEM characterization.

REFERENCES

1. Brunekreef, B.; Holgate, S. T., Air pollution and health. *Lancet* **2002,** *360* (9341), 1233-1242.

2. Bardouki, H.; Liakakou, H.; Economou, C.; Sciare, J.; Smolík, J.; Ždímal, V.; Eleftheriadis, K.; Lazaridis, M.; Dye, C.; Mihalopoulos, N., Chemical composition of size-resolved atmospheric aerosols in the eastern Mediterranean during summer and winter. *Atmos. Environ.* **2003,** *37* (2), 195-208.

3. Nel, A., Air Pollution-Related Illness: Effects of Particles. *Science* **2005,** *308*, 804-806.

4. Mahowald, N. Aerosol indirect effect on biogeochemical cycles and climate. Science **2011,** 334(6057), 794-796.

5. Horton, D. E.; Skinner, C. B.; Singh, D.; Diffenbaugh, N. S., Occurrence and persistence of future atmospheric stagnation events. *Nat. Clim. Change* **2014,** *4*, 698-703.

6. Zuo, F.; Zhang, S.; Liu, H.; Fong, H.; Yin, X.; Yu, J.; Ding, B., Free-Standing Polyurethane Nanofiber/Nets Air Filters for Effective PM Capture. *Small* **2017,** *13* (46), 1702139-1702150.

7. Xu, J.; Liu, C.; Hsu, P.-C.; Liu, K.; Zhang, R.; Liu, Y.; Cui, Y., Roll-to-Roll Transfer of Electrospun Nanofiber Film for High-Efficiency Transparent Air Filter. *Nano Lett.* **2016,** *16* (2), 1270-1275.

8. Liu, C.; Hsu, P.-C.; Lee, H.-W.; Ye, M.; Zheng, G.; Liu, N.; Li, W.; Cui, Y., Transparent air filter for high-efficiency PM2.5 capture. *Nat. Commun.* **2015,** *6*, 6205-6214.

9. Lv, D.; Zhu, M.; Jiang, Z.; Jiang, S.; Zhang, Q.; Xiong, R.; Huang, C., Green Electrospun Nanofibers and Their Application in Air Filtration. *Macromol. Mater. Eng.* **2018,** *303*,1800336-1800353.

10. Zhang, S.; Liu, H.; Yin, X.; Yu, J.; Ding, B., Anti-deformed Polyacrylonitrile/Polysulfone Composite Membrane with Binary Structures for Effective Air Filtration. *ACS Appl. Mater. Interfaces* **2016,** *8* (12), 8086-8095.

11. Sambaer, W.; Zatloukal, M.; Kimmer, D., 3D modeling of filtration process via polyurethane nanofiber based nonwoven filters prepared by electrospinning process. *Chem. Eng. Sci.* **2011,** *66* (4), 613-623.

12. Zhu, M.; Hua, D.; Pan, H.; Wang, F.; Manshian, B.; Soenen, S. J.; Xiong, R.; Huang, C., Green electrospun and crosslinked poly(vinyl alcohol)/poly(acrylic acid) composite membranes for antibacterial effective air filtration. *J. Colloid Interface Sci.* **2018,** *511*, 411-423.

13. Wan, H.; Wang, N.; Yang, J.; Si, Y.; Chen, K.; Ding, B.; Sun, G.; El-Newehy, M.; Al-Deyab, S. S.; Yu, J., Hierarchically structured polysulfone/titania fibrous membranes with enhanced air filtration performance. *J. Colloid Interface Sci.* **2014,** *417*, 18-26.

14. Wang, Z.; Zhao, C.; Pan, Z., Porous bead-on-string poly(lactic acid) fibrous membranes for air filtration. *J. Colloid Interface Sci.* **2015,** *441*, 121-129.

15. Li, Q.; Xu, Y.; Wei, H.; Wang, X., An electrospun polycarbonate nanofibrous membrane for high efficiency particulate matter filtration. *RSC Adv.* **2016,** *6* (69), 65275-65281.

16. Zhang, R.; Liu, C.; Hsu, P. C.; Zhang, C.; Liu, N.; Zhang, J.; Lee, H. R.; Lu, Y.; Qiu, Y.; Chu, S.; Cui, Y., Nanofiber Air Filters with High-Temperature Stability for Efficient PM2.5 Removal from the Pollution Sources. *Nano Lett.* **2016,** *16* (6), 3642-3649.

17. Nthunya, L. N.; Masheane, M. L.; Malinga, S. P.; Nxurnalo, E. N.; Barnard, T. G.; Kao, M.; Tetana, Z. N.; Mhlanga, S. D., Greener Approach To Prepare Electrospun Antibacterial beta-Cyclodextrin/Cellulose Acetate Nanofibers for Removal of Bacteria from Water. *ACS Sustain. Chem. Eng.* **2017,** *5* (1), 153-160.

18. Pangon, A.; Saesoo, S.; Saengkrit, N.; Ruktanonchai, U.; Intasanta, V., Multicarboxylic acids as environment-friendly solvents and in situ crosslinkers for chitosan/PVA nanofibers with tunable physicochemical properties and biocompatibility. *Carbohydr. Polym.* **2016,** *138*, 156-165.

19. Zhang, B.; Yan, X.; He, H.-W.; Yu, M.; Ning, X.; Long, Y.-Z., Solvent-free electrospinning: opportunities and challenges. *Polym. Chem.* **2017,** *8* (2), 333-352.

20. Jiang, S.; Hou, H.; Agarwal, S.; Greiner, A., Polyimide Nanofibers by "Green" Electrospinning via Aqueous Solution for Filtration Applications. *ACS Sustain. Chem. Eng.* **2016,** *4* (9), 4797-4804.

21. Giebel, E.; Mattheis, C.; Agarwal, S.; Greiner, A., Chameleon Nonwovens by Green Electrospinning. *Adv. Funct. Mater.* **2013,** *23* (25), 3156-3163.

22. Nicosia, A.; Gieparda, W.; Foksowicz-Flaczyk, J.; Walentowska, J.; Wesolek, D.; Vazquez, B.; Prodi, F.; Belosi, F., Air filtration and antimicrobial capabilities of electrospun PLA/PHB containing ionic liquid. *Sep. Purif. Technol.* **2015,** *154*, 154-160.

23. Celebioglu, A.; Uyar, T., Green and one-step synthesis of gold nanoparticles incorporated into electrospun cyclodextrin nanofibers. *Rsc Adv.* **2013,** *3* (26), 10197-10201.

24. Choi, D. Y.; Jung, S.-H.; Song, D. K.; An, E. J.; Park, D.; Kim, T.-O.; Jung, J. H.; Lee, H. M., Al-Coated Conductive Fibrous Filter with Low Pressure Drop for Efficient Electrostatic Capture of Ultrafine Particulate Pollutants. *ACS Appl. Mater. Interfaces* **2017,** *9* (19), 16495-16504.

25. Zhang, Y.; Yuan, S.; Feng, X.; Li, H.; Zhou, J.; Wang, B., Preparation of Nanofibrous Metal–Organic Framework Filters for Efficient Air Pollution Control. *J. Am. Chem. Soc.* **2016,** *138* (18), 5785-5788.

26. Zhu, J.; Lin, X.; Zhang, Z.; Luo, X., Preparation and characterization of KGM-g-St/BA fibers and core/shell PCL/KGM-g-St/BA fibers. *Rsc Adv.* **2015,** *5* (32), 24975-24983.

27. Wang, L.; Mu, R.-J.; Yuan, Y.; Gong, J.; Ni, Y.; Wang, W.; Pang, J., Novel nanofiber membrane fabrication from konjac glucomannan and polydopamine via electrospinning method. *J. Sol-Gel Sci. Technol.* **2018,** *85* (2), 253-258.

28. Ozgur, U.; Alivov, Y. I.; Liu, C.; Teke, A.; Reshchikov, M. A.; Dogan, S.; Avrutin, V.; Cho, S. J.; Morkoc, H., A comprehensive review of ZnO materials and devices. *J. Appl. Phys.* **2005,** *98* (4), 041301-041403.

29. Ibrahim, N. A.; Eid, B. M.; El-Aziz, E. A.; Abou Elmaaty, T. M.; Ramadan, S. M., Multifunctional cellulose-containing fabrics using modified finishing formulations. *RSC Adv.* **2017,** *7* (53), 33219-33230.

30. Ibrahim, N. A.; Eid, B. M.; El-Aziz, E. A.; Elmaaty, T. M. A.; Ramadan, S. M., Loading of chitosan – Nano metal oxide hybrids onto cotton/polyester fabrics to impart permanent and effective multifunctions. *Int. J. Biol. Macromol* **2017,** *105*, 769-776.

31. Ibrahim, N. A.; Eid, B. M., In *Handbook of Textile Effluent Remediation*; Yusuf, M. Eds.; New York: Pan Stanford, 2018; Chapter 7, pp 185-202.

32. Sheng, J.; Zhang, M.; Xu, Y.; Yu, J.; Ding, B., Tailoring Water-Resistant and Breathable Performance of Polyacrylonitrile Nanofibrous Membranes Modified by Polydimethylsiloxane. *ACS Appl. Mater. Interfaces* **2016,** *8* (40), 27218-27226.

33. Zhao, X.; Li, Y.; Hua, T.; Jiang, P.; Yin, X.; Yu, J.; Ding, B., Low-Resistance Dual-Purpose Air Filter Releasing Negative Ions and Effectively Capturing PM2.5. *ACS Appl. Mater. Interfaces* **2017,** *9* (13), 12054-12063.

34. Zhu, M.; Han, J.; Wang, F.; Shao, W.; Xiong, R.; Zhang, Q.; Pan, H.; Yang, Y.; Samal, S. K.; Zhang, F.; Huang, C., Electrospun Nanofibers Membranes for Effective Air Filtration. *Macromol. Mater. Eng.* **2017,** *302* (1), 1600353-1600380.

35. Sun, J.-X.; Yuan, Y.-P.; Qiu, L.-G.; Jiang, X.; Xie, A.-J.; Shen, Y.-H.; Zhu, J.-F., Fabrication of composite photocatalyst g-C3N4–ZnO and enhancement of photocatalytic activity under visible light. *Dalton Trans.* **2012,** *41* (22), 6756-6763.

36. Kansal, S. K.; Singh, M.; Sud, D., Studies on photodegradation of two commercial dyes in aqueous phase using different photocatalysts. *J. Hazard. Mater.* **2007,** *141* (3), 581-590.

Table of Contents